Research Square

Preprints are preliminary reports that have not undergone peer review. They should not be considered conclusive, used to inform clinical practice, or referenced by the media as validated information.

Chemistry in cryogenic etching: A tutorial

Remi Dussart

remi.dussart@univ-orleans.fr

Groupe de Recherches sur l'Énergétique des Milieux Ionisés

Gaelle Antoun

Groupe de Recherches sur l'Énergétique des Milieux Ionisés

Thomas Tillocher

Groupe de Recherches sur l'Énergétique des Milieux Ionisés

Loic Becerra

Groupe de Recherches sur l'Énergétique des Milieux Ionisés

Philippe Lefaucheux

Groupe de Recherches sur l'Énergétique des Milieux Ionisés

Research Article

Keywords:

Posted Date: October 20th, 2025

DOI: https://doi.org/10.21203/rs.3.rs-7623847/v1

License: This work is licensed under a Creative Commons Attribution 4.0 International License.
Read Full License

Additional Declarations: No competing interests reported.

Chemistry in cryogenic etching: A tutorial

Remi Dussart*, Gaelle Antoun, Thomas Tillocher, Loic Becerra, Philippe Lefaucheux

GREMI, Orléans University-CNRS, 14 Rue d'Issoudun BP 6744, 45067 Orléans, France

* remi.dussart@univ-orleans.fr

Abstract

Cooling the substrate to stimulate chemical reactions can seem rather counterintuitive. However, this is one of the advantages often observed in plasma cryogenic etching. This article discusses the interactions between plasma and the surface at low temperature. It begins by reviewing the fundamental theories of adsorption as applied to etching. The theoretical concepts are then illustrated in the second part of the article by two different cryogenic processes developed and studied as part of research programs: the reinforcement of the SiO_xF_y passivation layer in the STiGer cryogenic deep silicon etching process and cryogenic Atomic Layer Etching (cryo-ALE) of SiO_2 from physisorbed C_4F_8 molecules.

1. Introduction

Cooling the substrate for silicon etching was proposed for the first time in 1988 [1]. The idea was to freeze chemical reactions on the sidewalls of silicon trenches in an SF_6 plasma to promote anisotropy. A few years later, it was shown that a passivation mechanism with oxygen was necessary to achieve anisotropic etching [2]. Instead of freezing the chemical reactions, the very low temperature (-120°C) actually favored them at the sidewalls to form a SiO_xF_y layer, stable at low temperatures only, which was responsible for protecting the sidewalls from etching. The role of SiF_4 molecules, which are the main by-products in silicon etching with SF_6 plasma was highlighted and SiF_4/O_2 plasma was used to reinforce the passivation layer in the so-called STiGer process [3]. The passivation reinforcement was only efficient at low temperature of the substrate.

Cooling the substrate to promote chemical reactions seems counterintuitive. However, this behavior has been reported in numerous experiments conducted by the cryochemistry community long ago [4, 5]. Chemical reactions at low temperature are also studied by the planetology community [6, 7]. As explained in [5], in a freezing solution containing water and another substance, micro-pockets can form while ice crystals can form in the solution. During the solidification process, the volume occupied by the micropockets decreases and the concentration of the substance in the micropockets increases significantly. This concentration effect during solution solidification can accelerate chemical reactions, although the rate coefficient decreases with temperature, in accordance with Arrhenius' law. In cryogenic etch processes, the concentration is achieved at the surface at low temperature, increasing the residence time of the incident species at the surface.

Cryogenic etching processes have also been developed for different purposes such as ultra low-K etching without damage [8–10] and for ALE [11, 12] taking advantage of the enhanced physisorption of certain radicals at low temperature. More recently, HF/H_2O-based plasmas were successfully developed to etch, at low temperature, thin SiO_2 and Si_3N_4 layers alternatively stacked on silicon for 3D-NAND device applications [13]. Very high aspect ratio ONON (oxide-nitride) structures without defect were obtained demonstrating the very effective effect of the low temperature.

This article will focus on adsorption mechanisms at cryogenic temperatures, but not on the surface diffusion of adsorbed species, which can nevertheless play an important role in cryogenic etching. Readers interested in surface diffusion processes are invited to read article [14], which discusses these aspects in details.

The next section is dedicated to plasma surface interactions at low temperature, before describing and explaining some examples of physisorption and chemisorption mechanisms found in cryoetching.

2. Plasma surface interactions at low temperature

A plasma used for etching is usually very complex. Most of time, molecules containing halogen atoms are used to produce reactive radicals by dissociation. The numerous species produced by dissociation

complexify the control of the etching process since it is quite difficult to evaluate their individual concentration. In SF_6/O_2 plasma for example, F, S, SF, SF_x, SO_xF_y species are formed and it is very difficult, even by simulation, to have a reliable estimation of their concentration even in a global 0-D model at steady state. The etching by-products are also reinjected in the plasma and modify its composition, which makes the modeling even more complex. Moreover, many different ions, which may be positive or negative, are produced and usually play a crucial role in the etching process, allowing a synergetic effect that significantly increases the etch rate. In particular, at the surface of the substrate a space charge sheath forms, which is mainly composed of neutrals and positive ions. Positive ions gain most of their energy within this sheath, where they are accelerated by the large electric field that prevails in this region. In radio-frequency CCP (capacitively coupled plasma), note that electrons are also attracted every RF cycle during a very short time to discharge the surface and produce a net current per cycle equal to zero [15]. Two types of etching mechanisms are usually identified: chemical and physical etching. Chemical etching is due to spontaneous reactions of radicals with the molecules or atoms of the surface; Physical etching corresponds to the sputtering of the surface atoms by the impinging positive ions. In some cases, both mechanisms can combine to produce a synergetic effect, which can significantly enhance the etching rate.

In the case of chemical etching mechanism, reactive species have to be somehow trapped by the surface. This is what is called "adsorption". There are two types of adsorption: chemisorption and physisorption.

An illustration of chemisorption is provided in figure 1-a in the case of fluorine and oxygen radicals interacting with a silicon surface. In this case, radicals of the plasma that adsorb at the surface are called "adsorbates". They can "chemisorb" at the surface, which is composed of atoms or molecules called "adsorbent". The radicals make a strong covalent or ionic bond with the atoms or molecules of the surface, which has an energy as high as few electron-volts (eV). New molecules can be produced

at the surface, forming volatile by-products, which spontaneously leave the surface. Reactions can be endo- ($\Delta H>0$) or (most of cases) exo- thermic ($\Delta H<0$).

Species can also physisorb at the surface. An example is schematically provided in figure 1.b in the case of C_4F_8 molecules physisorption on a SiO_2 surface at low temperature. No reaction occurs, but molecules are stuck at the surface due to Van Der Waals interactions. The bond between physisorbed species and molecules of the surface is weak (< 0.5 eV). This process is favored at low temperature and can consequently play an important role in cryogenic etching.

The shape of the potential energy at the surface versus the distance between the adsorbate and the surface is represented in figure 1.c. (Lennard-Jones graph adapted from [14]). If a gas particle approaches the surface at a short distance (a few angstroms), it can be attracted and then repelled if it gets too close. There are two energy wells corresponding to physisorption and chemisorption.

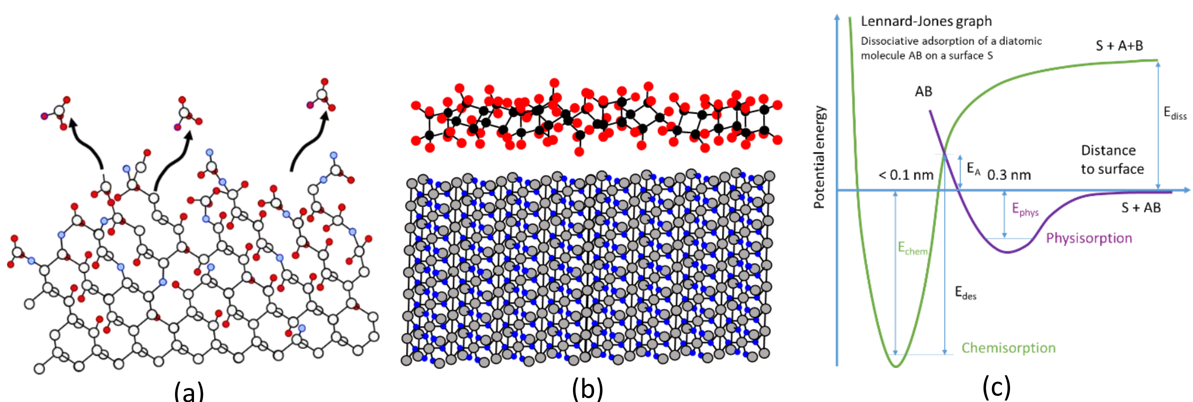

Figure 1: Illustration of (a) chemisorption of fluorine and oxygen species on a silicon surface in SF_6/O_2 plasma and (b) physisorption of C_4F_8 molecules on SiO_2 surface. Figure (c) is an example of Lennard-Jones graph, representing the potential energy versus distance to surface (adapted from T. Lill et al. [14])

As already mentioned, the physisorption well has a low desorption energy ($E_{phys} < 0.5$ eV) and appears at a greater distance than the chemisorption well, which is deeper ($E_{des} \approx$ few eV). Between the two, there is a potential barrier E_A, which is sometimes called Activation Energy. Physisorbed molecules or atoms must cross this potential barrier to be trapped by the chemisorption well. If not, they may be

released into the plasma without further interaction with the surface, after a certain amount of time, depending on the temperature of the adsorbent (surface). It should be noted that a diatomic molecule (AB in the diagram), which is initially physisorbed on the surface, may dissociate during the interaction and eventually reach the chemisorption well [14]. Two simple different models of adsorption are presented in the following paragraphs. However, it should be borne in mind that physisorption and chemisorption have complex mechanisms that can be described more accurately by quantum mechanics and statistical physics. If readers are interested by a deeper understanding of these aspects, they can read for example the book Physisorption Kinetics from H.J. Kreuzer and Z.W. Gortel [16].

2.1 The Langmuir model for monolayer adsorption

The Langmuir model is used to describe a layer surface coverage of a single monolayer [17]. Surface coverage θ is defined as the ratio between the number of occupied adsorption sites and the number of available adsorption sites. It relies on few assumptions: the surface must be flat at the atomic scale; a molecule or an atom can adsorb at a site without interacting with neighbor molecules at the surface. The Langmuir adsorption theory describes the balance between adsorption and desorption.

The rate of change of surface coverage is given by:

$$\frac{d\theta}{dt} = k_a\, pN(1-\theta) - k_d\, N\theta \tag{1}$$

Where N is the total number of sites; p is the pressure (in Pa); k_a and k_d are the rate constants for adsorption (in $Pa^{-1}.s^{-1}$) and desorption (in s^{-1}).

At equilibrium, we have $\frac{d\theta}{dt} = 0$, and equation (1) can be expressed as:

$$\theta = \frac{Kp}{1+Kp} \text{ with } K = \frac{k_a}{k_d} \tag{2}$$

An example of surface coverage is plotted versus pressure on figure 2. Such a curve is called isotherm because the temperature is supposed to be constant. It simply tells that the surface coverage increases as a function of pressure: it varies strongly at low pressure and more weakly at higher pressure.

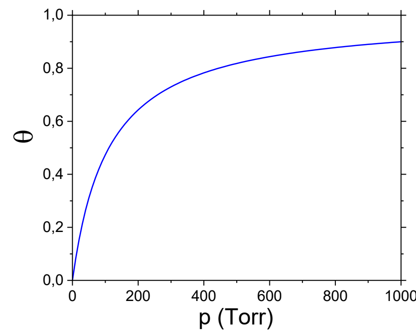

Figure 2: Example of Langmuir adsorption isotherm

2.1.1 Chemisorption

The Langmuir model seems adapted for the description of chemisorption mechanism during etching. Chemisorbed species react with the surface and produce molecules that leave the surface, so that the surface coverage remains below 1. However, in the case of etching, the desorbed species are different from adsorbed species and the surface evolves in time. Even if a steady state can be reached, it does not correspond to an equilibrium (reversible) state. However, a simple model, taken from [18] can be used to evaluate the etch rate. First, we can evaluate the spontaneous etching rate (ER_n) due to chemical reactions with incident reactive neutrals at the surface.

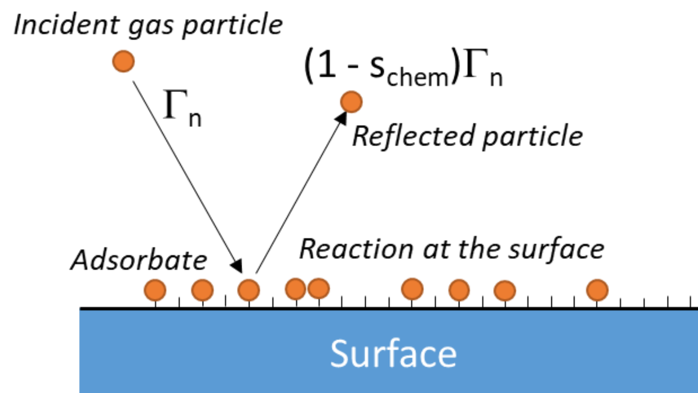

Figure 3: Sketch representing the chemisorption kinetic principle

If n is the density of reactive neutrals, having a Maxwell-Boltzmann distribution, one can evaluate the flux Γ_n of species hitting the surface:

$$\Gamma_n = \frac{1}{4} n v_n = \frac{P}{\sqrt{2\pi m k_B T}} \tag{3}$$

Reactive species can react (chemisorb) at the available sites of the surface with a certain probability s_{chem}, which represents the immediate sticking upon impact to form a chemical bond. The flux Γ_{nS} of species that will react with the surface is proportional to s_{chem} and the ratio of non-occupied sites $(1 - \theta)$.

$$\Gamma_{nS} = s_{chem}(1 - \theta)\Gamma_n = \frac{s_{chem}(1 - \theta)P}{\sqrt{2\pi m k_B T}} \tag{4}$$

The etching rate can be obtained by multiplying this flux by the etched volume V_e per reacting neutral.

$$ER_n = \frac{V_e\, s_{chem}(1 - \theta)P}{\sqrt{2\pi m k_B T}} \tag{5}$$

Of course, this is a very simple model for which a reactive species, which reacts at the surface would produce a volatile molecule that will spontaneously leave the surface. In reality, more than one species are usually necessary to form the volatile species and s_{chem} does not have the same value if a site of etching is partially occupied. In section 2, values of s_{chem} will be presented with fluorinated species interacting with SiF_x sites. This model could be used if etching products are mostly formed by spontaneous reaction of reactive neutrals with the surface. But, as already mentioned, in many cases such as Si etching by Cl_2 plasma, a synergetic effect is observed showing that spontaneous etching is assisted by ion bombardment. The etching rate ER_i due to both ion bombardment is then proportional to the ion energy E_i and to the ion flux Γ_i. It has also to be proportional to the surface coverage θ since the occupied sites will be preferentially sputtered in this case.

$$ER_i = k\theta E_i \Gamma_i \tag{6}$$

With k the volume removed per unit bombardment energy for a saturated surface ($\theta = 1$).

Equation (6) gives another expression of the etch rate. A first expression of the etch rate was provided by equation (5).

By equating these 2 expressions of ER, we can infer the expression for θ:

$$\theta = \frac{1}{1 + \frac{kE_i\Gamma_i\sqrt{2\pi m k_B T}}{V_e\, s_{chem} P}} \tag{7}$$

and, by reinjecting (7) in (6), we can finally have an expression of the etch rate:

$$ER = \frac{kE_i\Gamma_i}{1 + \frac{kE_i\Gamma_i\sqrt{2\pi m k_B T}}{V_e\, s_{chem} P}} \tag{8}$$

This expression of the etch rate describes well the synergetic effect between ion bombardment and spontaneous etching: if Γ_i is very low, the ER tends to zero; if the incident flux of reactive species is too low, the denominator of the ER becomes high and the ER tends to zero as well. Consequently, both reactive species and ion bombardment are necessary to reach a high etch rate. In this model driven by chemisorption and ion bombardment, a site which is occupied by a reactive species is not available anymore for another incident species, which is compatible with the Langmuir theory limited to one monolayer only. Chemisorption is optimal for a certain range of temperature. Indeed, if the incident species have a too low energy, they cannot cross the potential barrier E_A and get physisorbed. If the energy is too high, the species can just leave the chemisorption well.

2.1.2 Physisorption

The Langmuir theory can be used to describe physisorption, but only for the first deposited monolayer. A schematic of the principle of physisorption is shown in figure 4. In physisorption, incident species have a sticking probability "s" to occupy an available site of the surface. Then, they diffuse over the surface area and desorb after a certain time, which we will call "residence time at the surface".

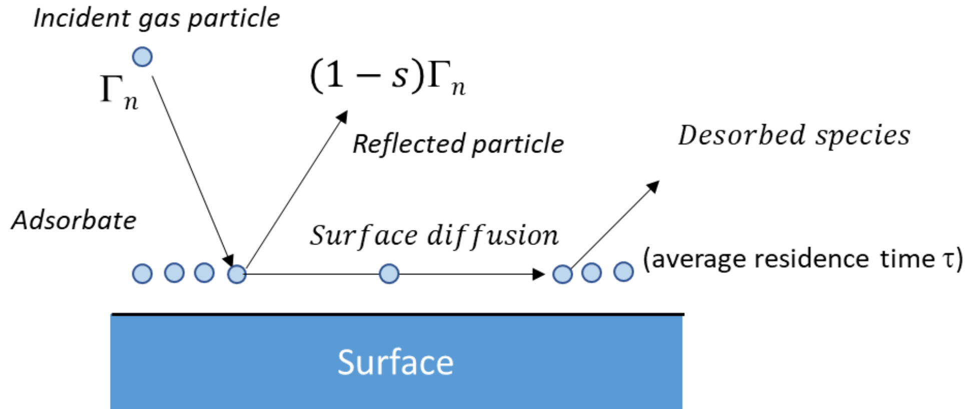

Figure 4: Sketch representing the physisorption kinetic principle

This residence time at the surface can be estimated using the Frenkel-Arrhenius law [16]:

$$t_d = t_d^0 \exp(\frac{E_d}{k_B T}) \tag{9}$$

with t_d^0 the attempt time of the particle for desorption and E_d the desorption energy for a physisorbed species.

$\nu = \frac{1}{t_d^0}$ is the attempt frequency with which the physisorbed particle tries to escape from the physisorption well. As explained in [16], ν is typically of the order of 10^{12}-10^{13} s^{-1}, but it can drop below 10^{10} s^{-1} around and above monolayer coverage.

The rate of change of surface coverage is the addition of an adsorption term minus a desorption term, proportional to θ in a first order reaction [16]:

$$\frac{d\theta}{dt} = \frac{sP}{N_S\sqrt{2\pi m k_B T}} - \frac{\theta}{t_d} \tag{9}$$

N_S is the surface concentration of surface sites.

Note that both s and t_d usually depend on temperature T and coverage θ as well.

When the surface is completely covered, physisorption can still go on, but the adsorbent is different from the solid surface itself: It now corresponds to a layer formed by the adsorbed gas particles. The

model called BET, developed by Brunet, Elmer and Teller [19], can be used to characterize the multi-layer physisorption process.

2.2 The BET model for multilayer adsorption

In the case of physisorption, it is obvious that the adsorption process is not limited to a monolayer. When the surface is completely covered by a first monolayer, the physisorption process continues through adsorbate-adsorbate interactions. The BET model is an extension of the Langmuir theory, which is applied to each adsorbed layer characterized by a rate of coverage θ_i, i being the layer number starting from 0. A fraction of the adsorption surface may be free or covered by 1,2 or more atoms or molecules. A sketch is proposed in figure 5 to illustrate the mechanism. The first layer ($i = 0$) interacts directly with the surface, with the interaction energy $E_{d,0}$. Adsorption of the layer $i \neq 0$ is based on adsorbate-adsorbate interaction. The adsorption energy $E_{d,i}$ is similar for all the layer numbers $i \neq 0$. There is adsorption-desorption equilibrium between the layer i and the layer $i - 1$. The BET model is valid below the vapor pressure $P_0(T)$ curve. If we cross the vapor pressure curve, gas starts to condensate: there is no equilibrium anymore, but a phase change from gas to solid.

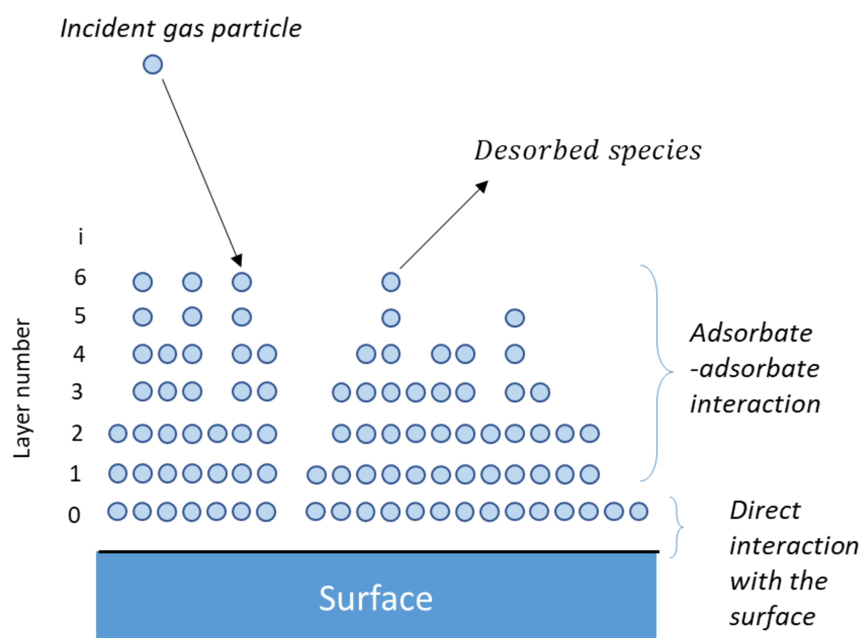

Figure 5: Sketch representing the BET multilayer adsorption

From these assumptions, it is possible to have the expression of θ_0 as a function of P. Then, by a recursive method, one can infer θ_i as a function of θ_0. After some additional calculations, the adsorbed gas amount υ can be found as a function of the adsorbed amount for one monolayer υ_m , $x = P/P_0$ and $C = e^{\frac{E_{d,0} - E_{d,i}}{k_B T}}$.

Knowing isotherm curves $\upsilon(x)$, it is possible to plot $\frac{x}{\upsilon(1-x)}$ as a function of x. A linear relationship should be obtained. The intercept and the slope are measured to determine υ_m, C and $\Delta E = E_{d,0} - E_{d,i}$.

An example of such a measure is presented in section 3.2.

3. Examples of physisorption and chemisorption in cryoetching processes

3.1. Cryoetching of silicon: role of SiF_x physisorption in the STiGer process

In standard deep cryoetching, a plasma of SF_6/O_2 with a low bias voltage (typically $|V_{bias}|$<60 V) is used to etch silicon while passivating the sidewalls to form vertical structures [20–22]. The passivation layer is composed of Si, F and O. The SiO_xF_y layer is quite fragile, but we showed that it could be reinforced by cyclic SiF_4/O_2 plasma steps. [3] This reinforcement effect is efficient at low temperature only.

What is the mechanism involved in this layer formation? S. Tinck et al. made molecular dynamic (MD) simulations to evaluate the sticking probability for chemisorption of various impinging species on different sites. The calculated values are reproduced in table 1. They showed that the values were not varying versus temperature in a wide range from -100°C to 27°C. [23]

Impinging species	on Si		on SiF		on SiF_2		on SiF_3	
	300 K	173 K	300 K	173 K	300 K	173 K	300 K	173 K
F	0.98	0.98	0.92	0.93	0.59	0.61	0.23	0.25
Si	1	1	1	1	0.41	0.40	0.20	0.19
SiF	0.88	0.89	0.49	0.50	0	0	0	0
SiF_2	0.51	0.50	0.18	0.19	0	0	0	0
SiF_3	0.37	0.37	0.06	0.06	0	0	0	0
SiF_4	0	0	0	0	0	0	0	0

F_2	1	1	1	1	0.77	0.77	0.3	0.31

Table 1: Calculated probabilities for immediate sticking upon impact of various impinging species (F, Si, SiF, SiF_2...) on different surfaces (Si, SiF, SiF_2 and SiF_3) (adapted from [24])

It can be concluded that reactions of fluorine and fluorinated silicon at the surface are not frozen in this range of temperatures, even at -100°C. Indeed, in pure SF_6 plasma, obtained profiles are isotropic regardless the temperature. An example of profiles obtained after 10 min of process in pure SF_6 plasma is shown in figure 6 at +30°C and -110°C. In these experimental conditions, there is no passivation layer formation and the cavities have similar dimensions

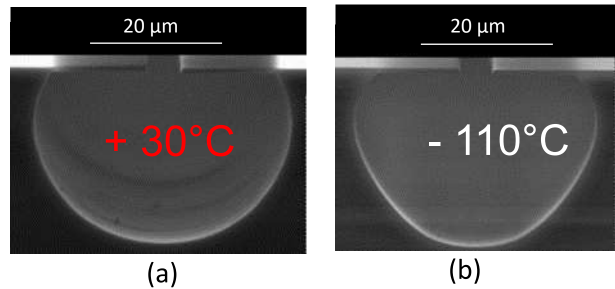

(a) (b)

Figure 6: Etched cavities obtained after 10 min of SF_6 plasma at 2 different temperatures: 30°C (a) and -110°C (b)

In the same paper of S. Tinck et al. [24], the authors calculated the physisorption energy of SiF_x species for 2 different temperatures (-100°C and 27°C). A significant change in the physisorption energy is observed at low temperature for SiF_4 and the SiF_x radicals on the different surfaces.

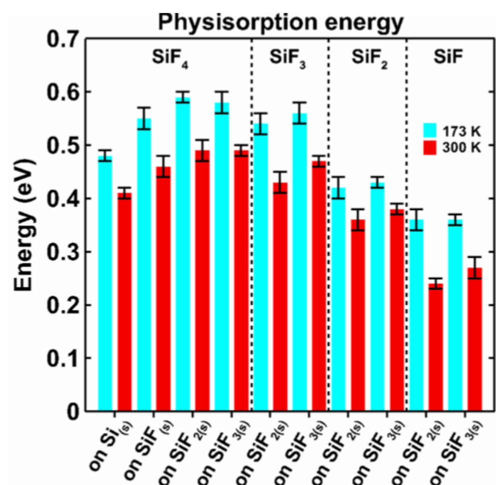

Figure 7: Sketch representing the BET multilayer adsorption

Using the equation (9) of section 2, they estimated the residence time of SiF_4 at the surface and found out that it was varying from 70 µs at room temperature to 960 s at -100°C [23]. Such a large change in residence time is expected for SiF_x species as well. This longer residence time of SiF_x at the surface can explain why the SiO_xF_y layer growth in SiF_4/O_2 plasma is more efficient at low temperature as reported in [25]. The probability of reaction between physisorbed species and impinging species is much higher at low temperature due the much longer residence time of the species. Here, physisorption of SiF_x species is followed by chemisorption with O and SiF_x radicals. The cold surface acts as a trap that captures reactive species on the surface and holds them there until another radical arrives and reacts with them. The formation of the passivation layer is a mixture of physisorption and chemisorption.

In-situ XPS analysis of the deposited SiO_xF_y layer after a SiF_4/O_2 plasma deposition step was carried at 3 different temperatures: -40°C, -65°C and -100°C. In the first column, the surface composition of the reference sample is provided before plasma. The composition is then given while maintaining the sample at low temperature during XPS analysis just after the plasma and then after heating to room temperature.

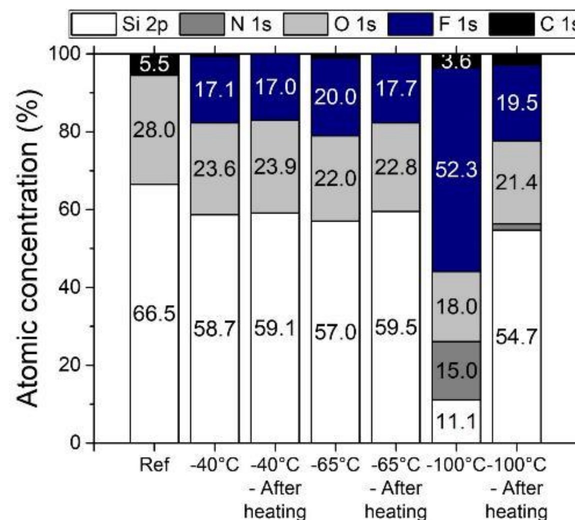

Figure 8: Composition of the a-Si surface obtained by in-situ XPS analysis after a plasma of SiF_4/O_2 at 3 different temperatures.
The composition of the sample before plasma is referred to as Ref (first column)
For each sample, the composition of the layer is shown while maintaining the sample at low temperature and after heating. (adapted from [26])

The surface composition is quite similar at -40°C and -65°C with about 17-20% of fluorine and 22-24% of oxygen. The composition does not vary much after heating when the process is performed at these two temperatures. At -100°C, the surface is significantly changed as compared to -40 and -65°C. The fluorine concentration reaches 52 %. However, when heating the sample, many species desorb from the surface, and the composition is again close to the one obtained at -40 and -65°C. We can conclude from these experiments that the deposited layer composition grown by SiF_4/O_2 plasma can be tuned by modifying the temperature of the substrate. This is due to a mixture of physisorption and chemisorption as already mentioned. This property was successfully used to define a cryo-ALE process based on a modification surface step at low temperature with SiF_4/O_2 plasma. [12]

3.2. Physisorption based cryo-ALE

A physisorption based cryo-ALE process was proposed to etch SiO_2 monolayer by monolayer. The cycle description is shown in figure 9. The idea is to inject a gas above the cold substrate to favor physisorption on one or few monolayers. The injection step is carried out without plasma. Then, the gas is replaced by Ar (purge). The following step is the Ar plasma to make physisorbed species react with the surface (chemisorption) and initiate etching at the monolayer scale. The cycle is then repeated.

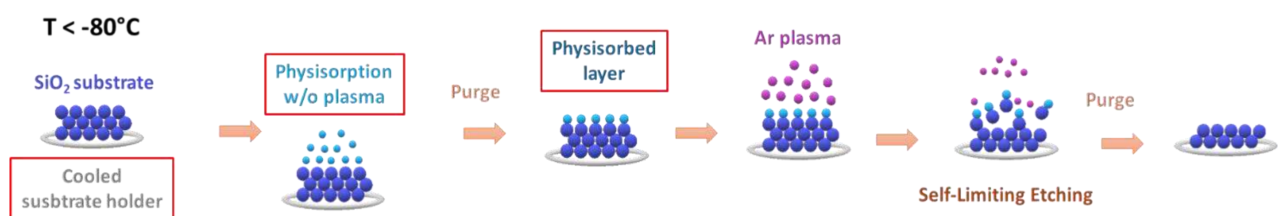

Figure 9: Description of the different steps used in Physisorption based cryo-ALE.

We used C_4F_8 gas for the physisorption step, as it is commonly used for SiO_2 etching [27].

In figure 10, the SiO_2 thickness time evolution is shown during 8 cycles for two different temperatures (-110 and -120°C). More details about the experiments can be found in [11].

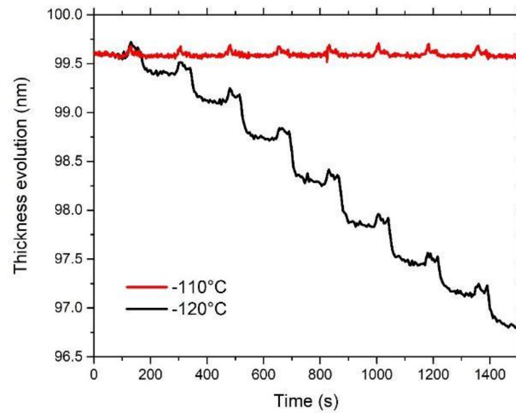

Figure 10: Thickness evolution versus time during 8 cycles of C_4F_8 physisorption based ALE at two temperatures: -110 and -120°C

At -110°C, no etching is observed. We can just observe some very slight thickness variations during the injection steps. At -120°C, these thickness variations due to injection steps are followed by etching with an Etch Per Cycle (EPC) of the order of one monolayer. It should be also noted that the Self-Limiting Etching (SLE) regime was reached. The question is: why is SiO_2 etching observed at -120°C, but not at -110°C? To answer this question, desorption analysis was carried out using mass spectrometry.

The results are shown in figure 11a showing the $C_2F_4^+$ peak signal (100 amu), which was monitored in Multiple Ion Detection (MID) mode by mass spectrometry. This line at 100 amu is the main line of the fragmentation spectrum of C_4F_8 in Residual Gas Analysis (RGA) at 70 eV. The C_4F_8 gas was injected during 1 min at 3 Pa on a SiO_2 wafer cooled to different temperatures between -112 and -122°C. During the C_4F_8 injection step, the $C_2F_4^+$ signal is high until the injection valve is closed. Then, a sharp drop of one or few orders of magnitude is logically observed on the signal. Then, for lower temperatures ($T \leq 114$°C), a plateau is observed during a certain time t_d, which corresponds to the desorption of C_4F_8 species from the surface. This desorption time increases when decreasing the surface temperature, in agreement with the residence time, which increases when the temperature is lowered. These desorption times were plotted in log scale as a function of 1000/T (figure 11.b). The data points can be fitted by a linear regression, which confirms the residence time dependence with temperature determined by equation 9.

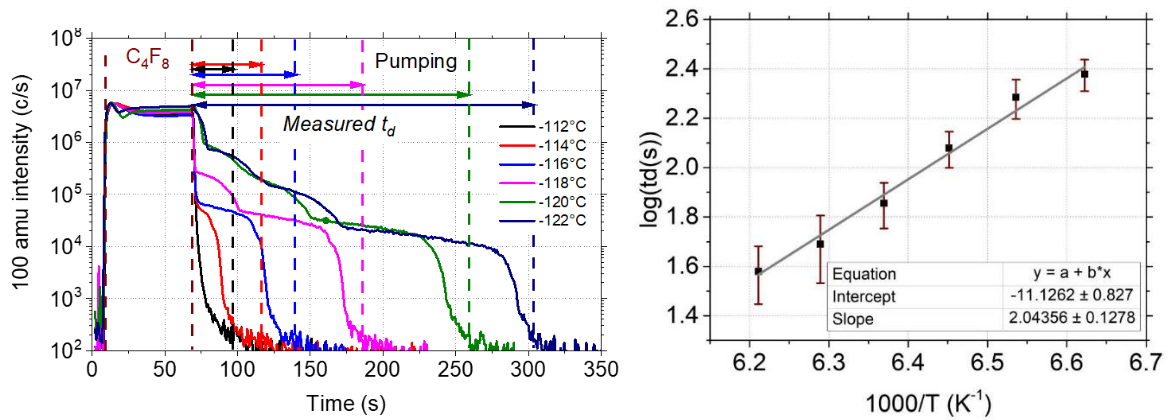

Figure 11: (a) $C_2F_4^+$ ion signal versus time when injecting C_4F_8 during 30s on a surface cooled down to a temperature between -112 and -122°C and after closing the gas injection valve.

(b) Graph of the residence time versus 1000/T. Data points are fitted using a linear regression.

From this plot, a desorption energy E_d as high as 0.404 eV and an attempt time t_d^0 of about 10^{-11} s could be deduced. [28]

By varying the pressure, adsorbed amount of C_4F_8 was measured by ellipsometry. The results are shown in figure 12a where the C_4F_8 thickness was evaluated versus time. The adsorbed amount ν was then plotted versus pressure normalized to the C_4F_8 vapor pressure P_0 at three different temperatures (figure 12b). An isotherm of type II [29, 30] is obtained and looks similar for the three temperatures.

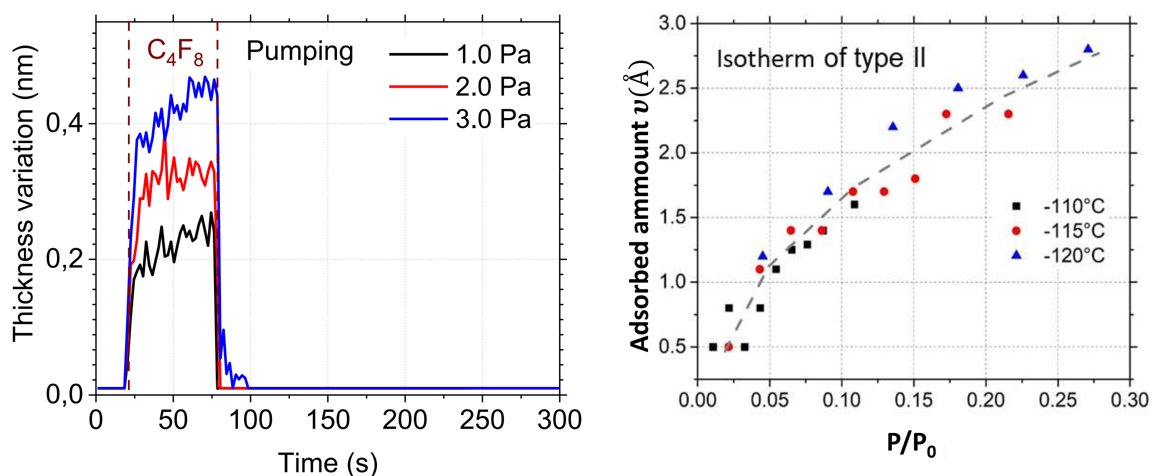

Figure 12: (a) C_4F_8 thickness versus time for three different pressures at -120°C. (b) C_4F_8 adsorbed amount versus P/P_0 for three different temperatures.

From the data points of figure 12(b), the ratio $\frac{x}{\upsilon(1-x)}$ was calculated and plotted versus $x = P/P_0$ following the method described in section 2.2. The data points are well fitted by linear regressions and curve slopes for the three temperatures are very similar. From these slopes and intercepts, we can determine $C = e^{\frac{E_{d,0}-E_{d,i}}{k_B T}}$ and υ_m. We found mean values of C= 19.8 ± 3.6 and υ_m = 2.2 ± 0.2 Å. From C mean value, we can estimate $\Delta E = E_{d,0} - E_{d,i}$, which is equal to 0.040± 0.001 eV.

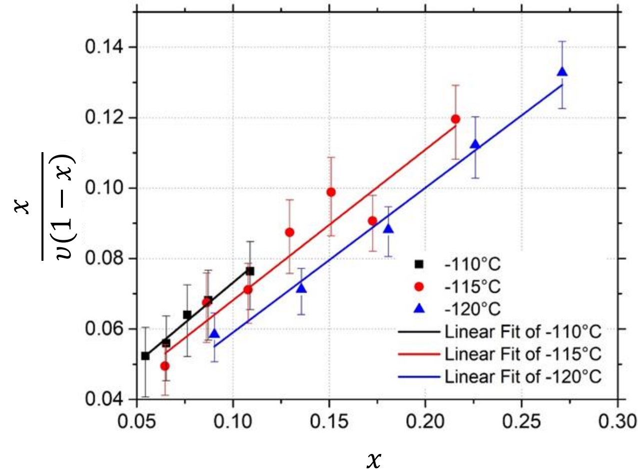

Figure 13: $\frac{x}{\upsilon(1-x)}$ plotted using data points of figure 12.b versus x for the three different temperatures

The ΔE value is close to typical ones found in literature [19]. From the value of $E_{d,0}$ = 0.404 eV, we deduce $E_{d,I}$=0.364 eV for C_4F_8-C_4F_8 physisorption.

4. Conclusions

The combination of both physisorption and chemisorption mechanisms play a significant role in cryogenic etching. In some cases, the cooled surface acts as a trap for species that have a much longer residence time at the surface and can react with other radicals from the plasma. This effect is found in both etching and deposition at low temperature and can significantly modify the composition of the deposited layer. Physisorption at very low temperature leads to multilayer adsorption where the desorption energy is different between the first and the following layers. Mass spectrometry measurements and spectroscopic ellipsometry can be used to evaluate the residence time of species

at the surface and the adsorbed amount. From these results, energy of desorption of the first monolayer and subsequent layers can be inferred by using the BET model, which describes well multilayer adsorption.

5. References

1. Tachi S, Tsujimoto K, Okudaira S (1988) Low-temperature reactive ion etching and microwave plasma etching of silicon. Applied Physics Letters 52:616–618. https://doi.org/10.1063/1.99382

2. Bartha JW, Greschner J, Puech M, Maquin P (1995) Low temperature etching of Si in high density plasma using SF6/O2. Microelectronic Engineering 27:453–456. https://doi.org/10.1016/0167-9317(94)00144-J

3. Tillocher T, Dussart R, Overzet LJ, et al (2008) Two Cryogenic Processes Involving SF[sub 6], O[sub 2], and SiF[sub 4] for Silicon Deep Etching. J Electrochem Soc 155:D187. https://doi.org/10.1149/1.2826280

4. McGee HA, Martin WJ (1962) Cryochemistry. Cryogenics 2:257–267. https://doi.org/10.1016/0011-2275(62)90001-2

5. An L-Y, Dai Z, Di B, Xu L-L (2021) Advances in Cryochemistry: Mechanisms, Reactions and Applications. Molecules 26:750. https://doi.org/10.3390/molecules26030750

6. Yu X, Zhao YS, Wu Y, et al (2023) Cryogenic Sulfuric Weathering and Challenges for Preserving Iron-Rich Olivine on Cold and Icy Mars. JGR Planets 128:e2022JE007593. https://doi.org/10.1029/2022JE007593

7. Malysheva LK, Malyshev AI (2021) Cryovolcanism and Degassing on Titan, a Moon of Saturn. J Volcanolog Seismol 15:201–215. https://doi.org/10.1134/S0742046321030040

8. Leroy F, Zhang L, Tillocher T, et al (2015) Cryogenic etching processes applied to porous low- *k* materials using SF_6 /C_4F_8 plasmas. J Phys D: Appl Phys 48:435202. https://doi.org/10.1088/0022-3727/48/43/435202

9. Zhang L, Ljazouli R, Lefaucheux P, et al (2013) Low Damage Cryogenic Etching of Porous Organosilicate Low-k Materials Using SF_6 /O_2 /SiF_4. ECS J Solid State Sci Technol 2:N131–N139. https://doi.org/10.1149/2.001306jss

10. Chanson R, Zhang L, Naumov S, et al (2018) Damage-free plasma etching of porous organo-silicate low-k using micro-capillary condensation above −50 °C. Sci Rep 8:1886. https://doi.org/10.1038/s41598-018-20099-5

11. Antoun G, Lefaucheux P, Tillocher T, et al (2019) Cryo atomic layer etching of SiO_2 by C_4F_8 physisorption followed by Ar plasma. Appl Phys Lett 115:153109. https://doi.org/10.1063/1.5119033

12. Antoun G, Tillocher T, Girard A, et al (2022) Cryogenic nanoscale etching of silicon nitride selectively to silicon by alternating SiF_4 /O_2 and Ar plasmas. Journal of Vacuum Science & Technology A 40:052601. https://doi.org/10.1116/6.0001885

13. Kihara Y, Tomura M, Sakamoto W, et al (2023) Beyond 10 μm Depth Ultra-High Speed Etch Process with 84% Lower Carbon Footprint for Memory Channel Hole of 3D NAND Flash over 400 Layers. In: 2023 IEEE Symposium on VLSI Technology and Circuits (VLSI Technology and Circuits). IEEE, Kyoto, Japan, pp 1–2

14. Lill T, Berry IL, Shen M, et al (2023) Dry etching in the presence of physisorption of neutrals at lower temperatures. Journal of Vacuum Science & Technology A 41:023005. https://doi.org/10.1116/6.0002230

15. Shin HC, Hu C (1996) Thin gate oxide damage due to plasma processing. Semicond Sci Technol 11:463–473. https://doi.org/10.1088/0268-1242/11/4/002

16. Kreuzer HJ, Gortel ZW, Toennies P (1986) Physisorption kinetics. Springer, Berlin

17. Langmuir I (1918) THE ADSORPTION OF GASES ON PLANE SURFACES OF GLASS, MICA AND PLATINUM. J Am Chem Soc 40:1361–1403. https://doi.org/10.1021/ja02242a004

18. Gottscho RA, Jurgensen CW, Vitkavage DJ (1992) Microscopic uniformity in plasma etching. Journal of Vacuum Science & Technology B: Microelectronics and Nanometer Structures Processing, Measurement, and Phenomena 10:2133–2147. https://doi.org/10.1116/1.586180

19. Brunauer S, Emmett PH, Teller E (1938) Adsorption of Gases in Multimolecular Layers. J Am Chem Soc 60:309–319. https://doi.org/10.1021/ja01269a023

20. Dussart R, Mellhaoui X, Tillocher T, et al (2007) The passivation layer formation in the cryo-etching plasma process. Microelectronic Engineering 84:1128–1131. https://doi.org/10.1016/j.mee.2007.01.048

21. Mellhaoui X, Dussart R, Tillocher T, et al (2005) SiOxFy passivation layer in silicon cryoetching. Journal of Applied Physics 98:104901. https://doi.org/10.1063/1.2133896

22. Dussart R, Tillocher T, Lefaucheux P, Boufnichel M (2014) Plasma cryogenic etching of silicon: from the early days to today's advanced technologies. J Phys D: Appl Phys 47:123001. https://doi.org/10.1088/0022-3727/47/12/123001

23. Tinck S, Neyts EC, Bogaerts A (2014) Fluorine–Silicon Surface Reactions during Cryogenic and Near Room Temperature Etching. J Phys Chem C 118:30315–30324. https://doi.org/10.1021/jp5108872

24. Tinck S, Neyts EC, Bogaerts A (2014) Fluorine–Silicon Surface Reactions during Cryogenic and Near Room Temperature Etching. J Phys Chem C 118:30315–30324. https://doi.org/10.1021/jp5108872

25. Antoun G, Dussart R, Tillocher T, et al (2019) The role of physisorption in the cryogenic etching process of silicon. Jpn J Appl Phys 58:SEEB03. https://doi.org/10.7567/1347-4065/ab1639

26. Antoun G, Girard A, Tillocher T, et al (2022) Quasi In Situ XPS on a $SiO_x F_y$ Layer Deposited on Silicon by a Cryogenic Process. ECS J Solid State Sci Technol 11:013013. https://doi.org/10.1149/2162-8777/ac4c7d

27. Metzler D, Li C, Engelmann S, et al (2016) Fluorocarbon assisted atomic layer etching of SiO2 and Si using cyclic Ar/C4F8 and Ar/CHF3 plasma. Journal of Vacuum Science & Technology A: Vacuum, Surfaces, and Films 34:01B101. https://doi.org/10.1116/1.4935462

28. Antoun G, Tillocher T, Lefaucheux P, et al (2021) Mechanism understanding in cryo atomic layer etching of SiO2 based upon C4F8 physisorption. Sci Rep 11:357. https://doi.org/10.1038/s41598-020-79560-z

29. Donohue MD, Aranovich GL (1998) Classification of Gibbs adsorption isotherms. Advances in Colloid and Interface Science 76–77:137–152. https://doi.org/10.1016/S0001-8686(98)00044-X

30. Sing KSW (1994) Physisorption of gases by carbon blacks. Carbon 32:1311–1317. https://doi.org/10.1016/0008-6223(94)90117-1

Funding Declaration

This research project is supported by the CERTeM scientific interest group (GIS), which provides most of the equipment and is funded by the European Union (FEDER fund) as well as the French National Research Agency (ANR PSICRYO fund for “Understanding Plasma-Surface Interactions in CRYOgenic etching for advanced patterning applications”; No. ANR-20-CE24-0014).